Supplement of Atmos. Chem. Phys., 20, 881–899, 2020
https://doi.org/10.5194/acp-20-881-2020-supplement

Atmospheric Chemistry and Physics
Open Access

Supplement of

Air pollution slows down surface warming over the Tibetan Plateau

Aolin Jia et al.

Correspondence to: Shunlin Liang (sliang@umd.edu)

S1. Data

S1.1 Surface air temperature datasets

Table S1 (Rao *et al.*, 2018). Meta information on the four surface air temperature datasets. All datasets were resampled into 1 Lat/Lon degree, and the climatology periods were transferred to 1961–1990 in the paper. All data were accessed on 20 July 2018.

Data	Spatial Resolution	Climatology Period	No. of Sites	Homogenization method	Interpolation method	Data Availability	Notes
BEST-LAND	1°×1°	1951–1980	36866	scalpel: Split time series using detected break points and automatically adjust weight for each time series	Gaussian process regression/ Kriging	http://berkeleyearth.org/data/	Muller et al. (2013a) and Rohde et al. (2013b)
CRU-TEM4v	5°×5°	1961–1990	5583	Comparing with neighbor stations	No interpolation implemented	http://www.cru.uea.ac.uk/data	Jones et al. (2012)
NASA-GISS	2°×2°	1951–1980	7290	Comparing with neighbor stations; urbanization adjustment	Distance-dependent weighted average of station observations within a 1200-km radius	https://data.giss.nasa.gov/gistemp/	Hansen et al. (2010)
NOAA-NCEI	5°×5°	1961–1990	7280	Comparing with neighbor stations	Two-step (low and high frequency) reconstruction using Empirical Orthogonal Teleconnection	https://governmentshutdown.noaa.gov/	Smith et al. (2008) and Vose et al. (2012)

S2. Supplementary Results

S2.1 CERES EBAF Surface Downward Shortwave Radiation Assessment

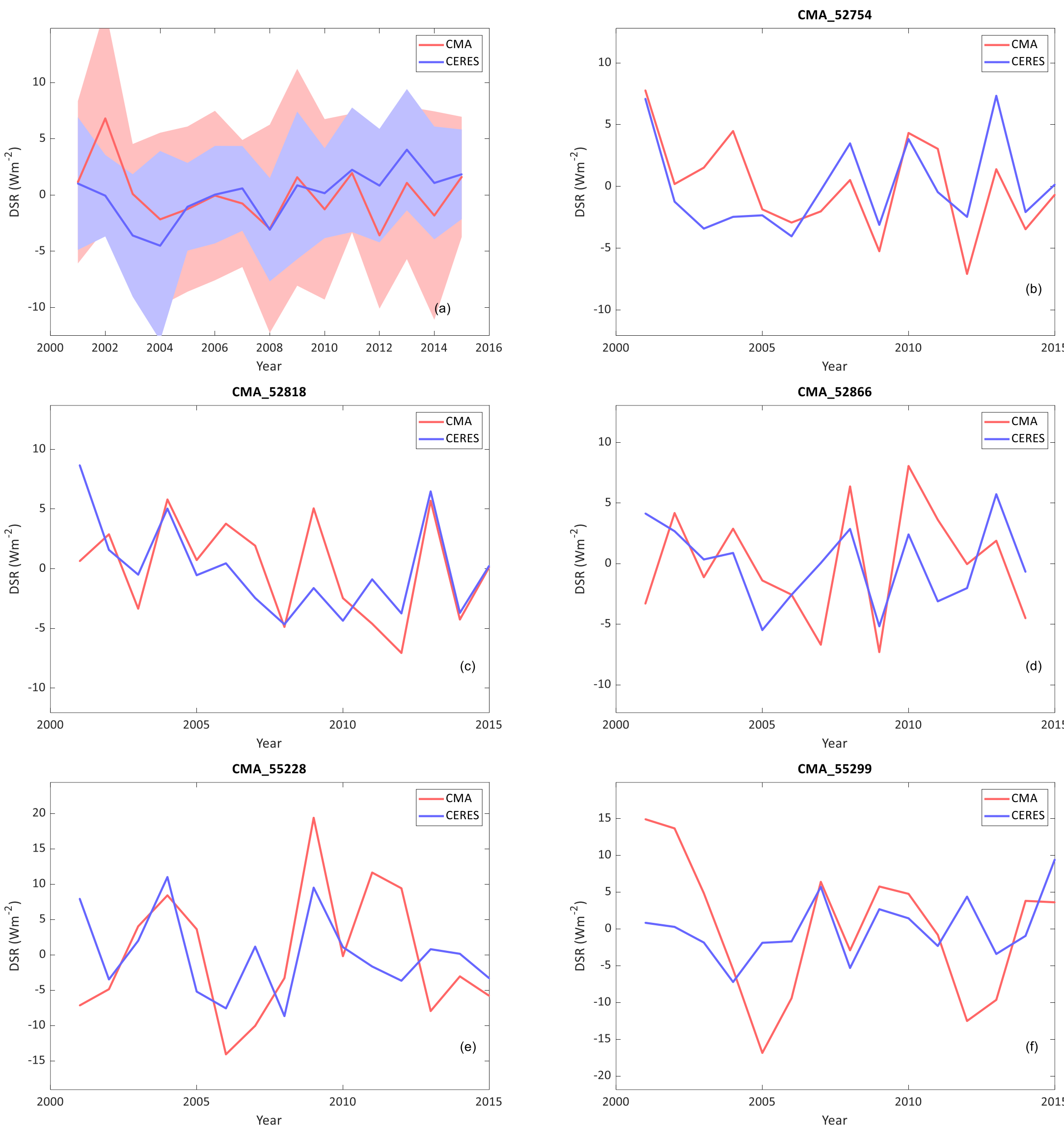

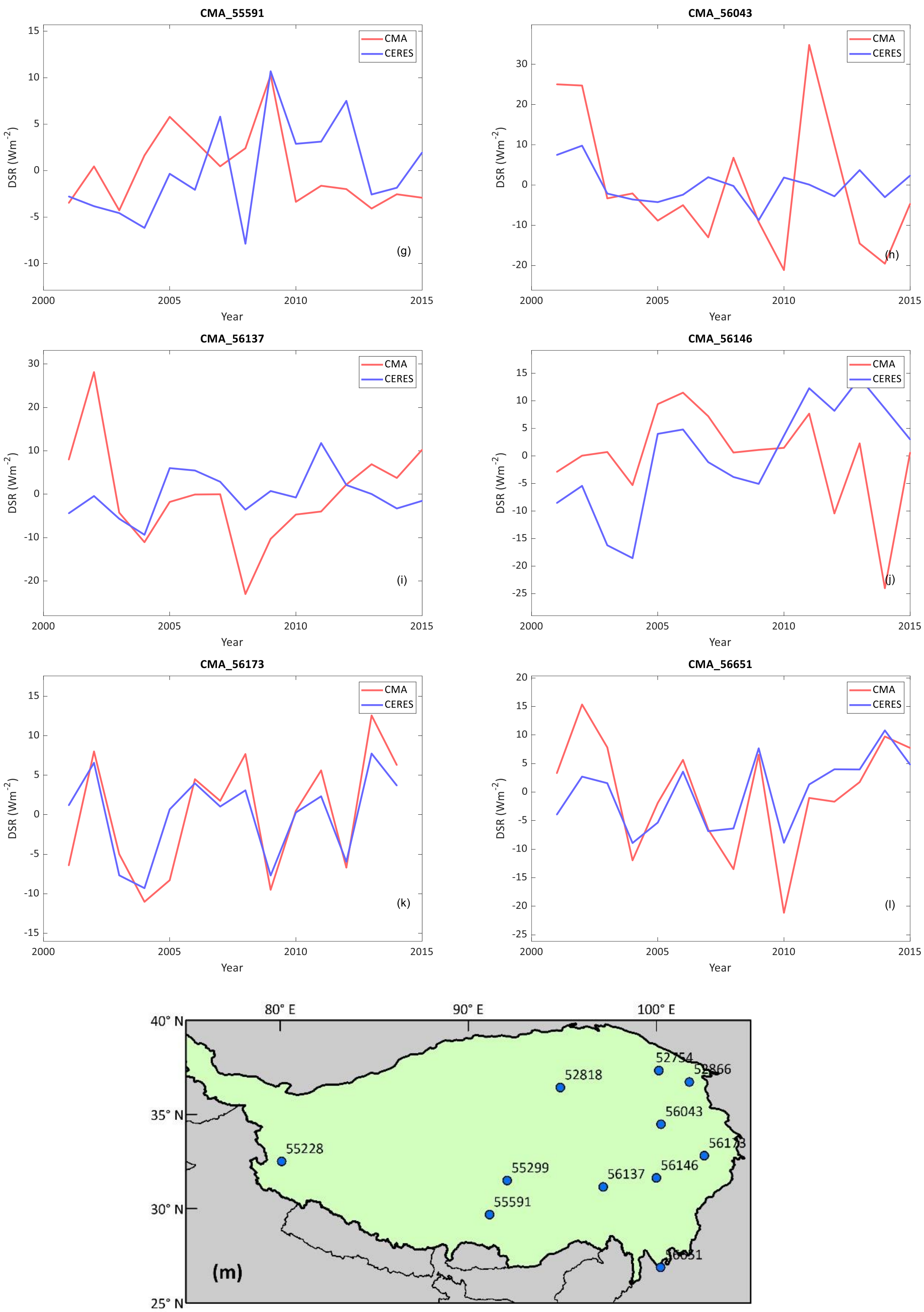

Fig. S1: Surface DSR temporal variation of CERES and all CMA radiation sites at TP (a) 11 CMA sites mean, (b-l) individual sites, and (m) 11 sites distribution.

S2.2 Analysis of Long-Term Surface Downward Solar Radiation Measurements since 1958

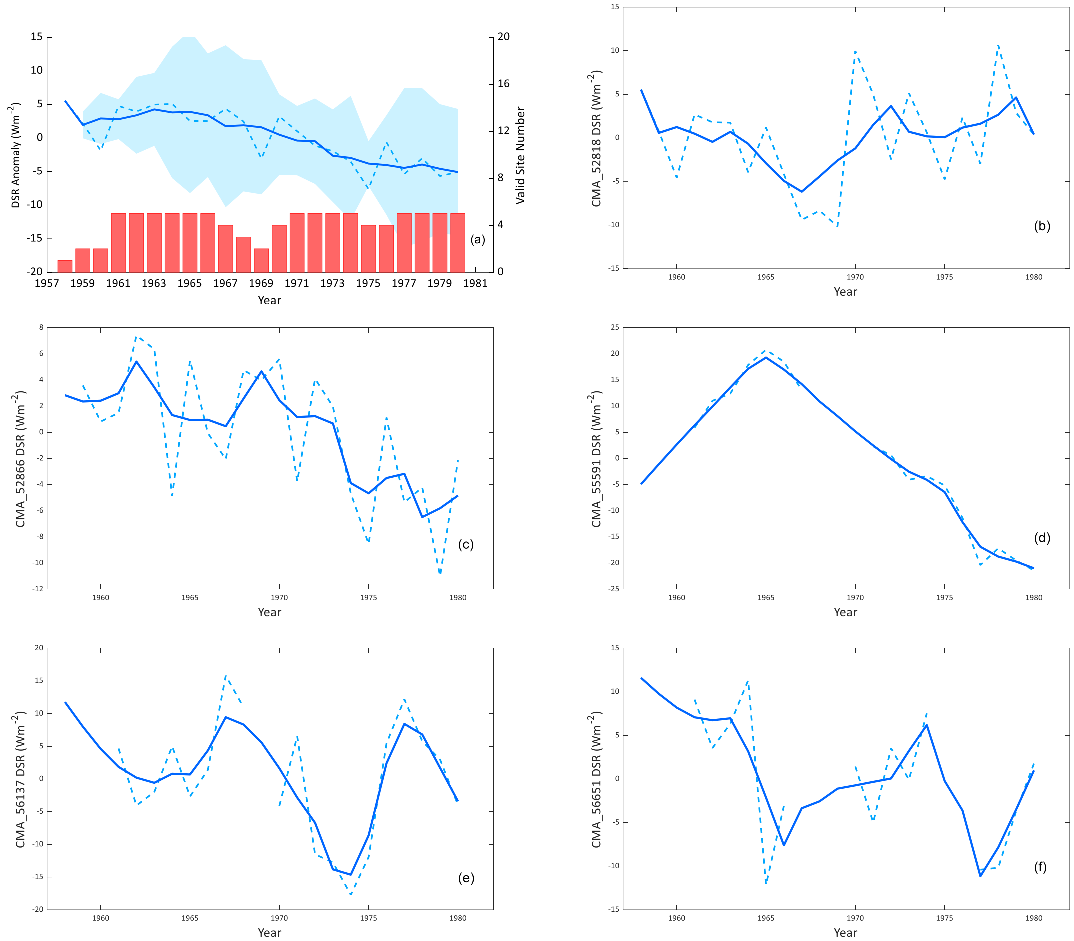

Fig. S2: Surface DSR temporal variation of (a) 5 CMA sites mean, (b-f) individual sites. Temporal variations were averaged by the 5-year moving window in order to remove the impact of annual variability. Observations after 1980 were abandoned due to the data discontinuity.

S2.3 Analysis of Deep Convective Clouds and Atmospheric Water Vapor

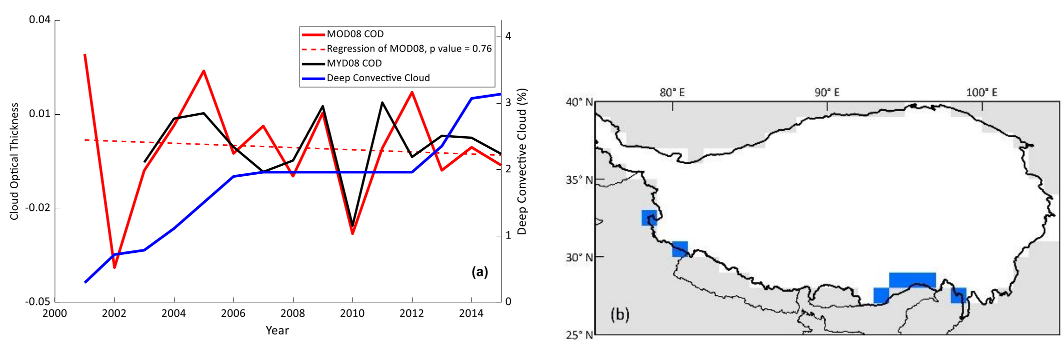

Fig. S3: (a) Temporal variation of the cloud optical depth and deep convective clouds from the MODIS 08 products; (b) Deep convective cloud distribution over the TP. The blue pixels are the location of the deep convective cloud once it appeared.

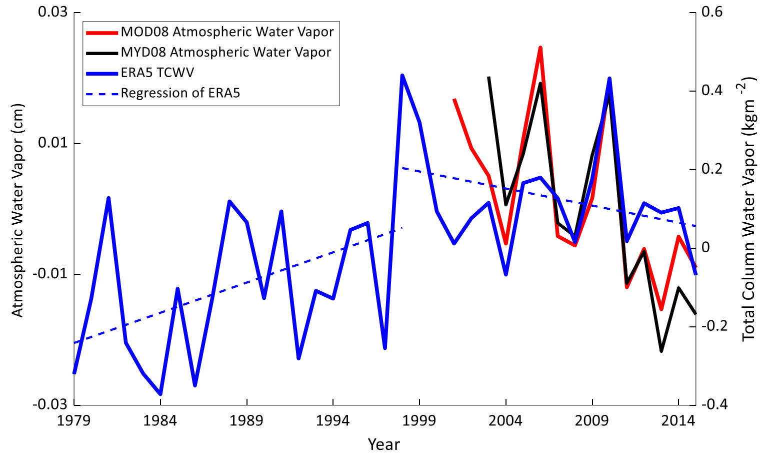

Fig. S4: Temporal annual variation of the atmospheric water vapor from MODIS atmospheric products and ERA5. ERA5 shows a considerable turning point in 1998 and the decreasing trend matches with satellite products very well. The *p* value of the regression in 1979-1998 (1999 - 2015) is 0.04 and 0.10.

S2.4 Aerosol data analysis

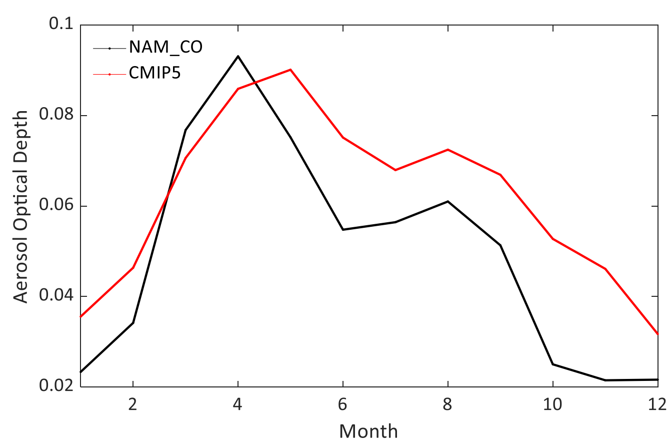

Figure S5: Monthly climatology of aerosol optical depth from the CMIP5 estimation and AERONET(AErosol RObotic NETwork) NAM_CO site observation.

S2.5 Radiative Forcing of Anthropogenic Aerosols

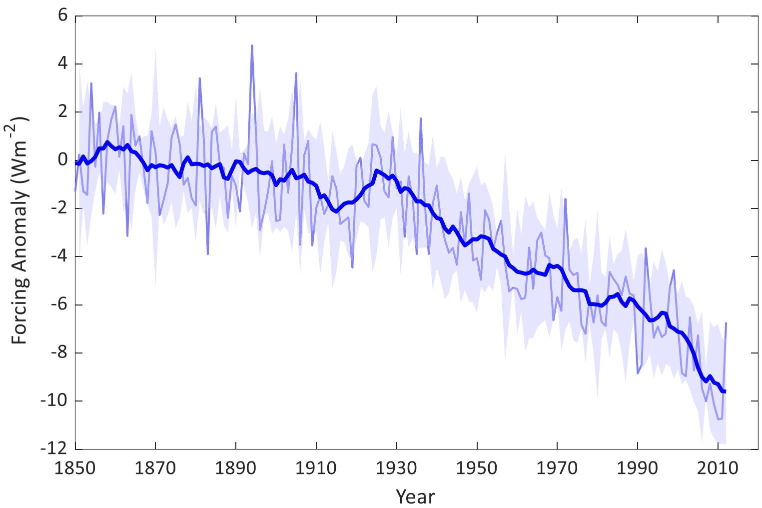

Fig. S6: Temporal variation in the aerosol radiative forcing anomalies. The shaded area is the standard deviation of model average.

S2.6 Depressing Effect Calculated by Two Methods

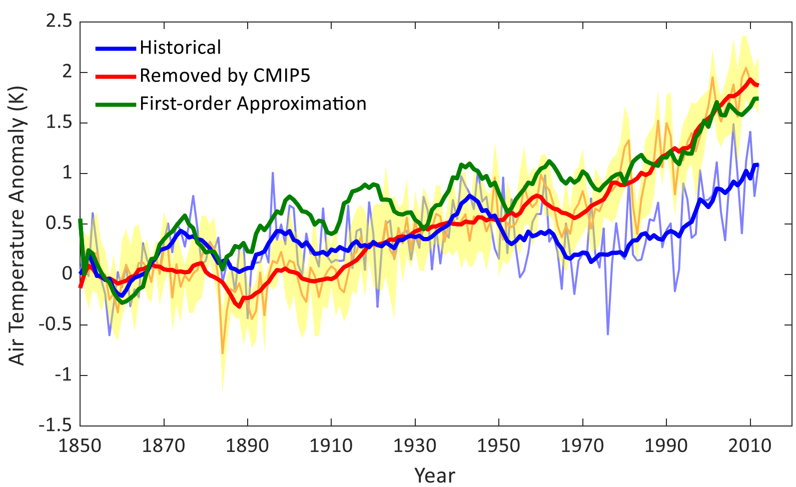

Fig. S7: The temporal annual variation in air temperature, and air temperature with the depressing effect of aerosols removed in the summer season, using two methods. The shaded area is the standard deviation of model average.

S2.7 Surface and TOA Variable Analysis

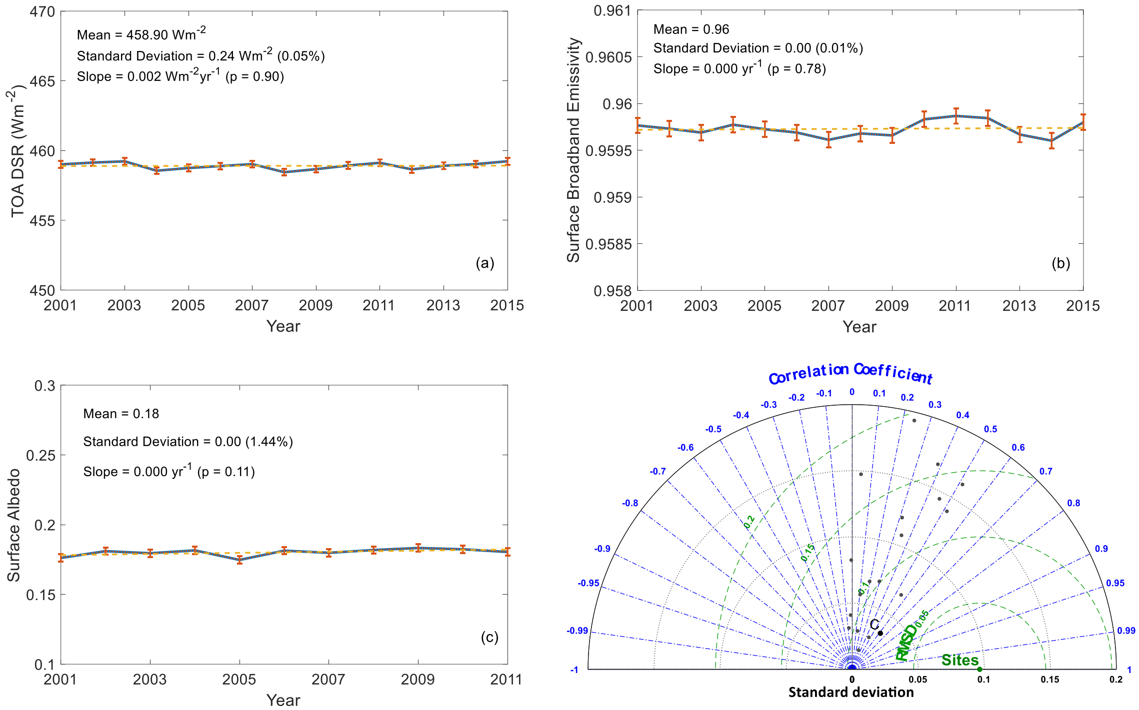

Fig. S8: (a - c) The temporal annual variation in TOA DSR, surface broadband emissivity, and surface albedo over the TP in the summer season. The Figures show stable variation of the three variable. (d) Taylor diagram of solar validation of CERES EBAF (black dot C) and 18 CMIP5 models (grey dots) based on CAMP network. The result shows combined albedo satellite product has higher accuracy than individual model simulations.

References

Hansen, J., R. Ruedy, M. Sato, and K. Lo (2010), Global surface temperature change, Reviews of Geophysics, 48(4).

Jones, P., D. Lister, T. Osborn, C. Harpham, M. Salmon, and C. Morice (2012), Hemispheric and large‐scale land‐surface air temperature variations: An extensive revision and an update to 2010, Journal of Geophysical Research: Atmospheres, 117(D5).

Rao, Y., S. Liang, and Y. Yu (2018), Land Surface Air Temperature Data Are Considerably Different Among BEST-LAND, CRU-TEM4v, NASA-GISS, and NOAA-NCEI, Journal of Geophysical Research: Atmospheres, 123(11), 5881-5900, doi: 10.1029/2018jd028355.

Rohde, R., R. Muller, R. Jacobsen, E. Muller, S. Perlmutter, A. Rosenfeld, J. Wurtele, D. Groom, and C. Wickham (2013a), A new estimate of the average Earth surface land temperature spanning 1753 to 2011. Geoinfor Geostat Overview 1: 1, of, 7, 2.

Rohde, R., R. Muller, R. Jacobsen, S. Perlmutter, A. Rosenfeld, J. Wurtele, J. Curry, C. Wickhams, and S. Mosher (2013b), Berkeley Earth Temperature Averaging Process. Geoinfor Geostat: An Overview 1: 2, of, 13, 20-100.

Smith, T. M., R. W. Reynolds, T. C. Peterson, and J. Lawrimore (2008), Improvements to NOAA's historical merged land–ocean surface temperature analysis (1880–2006), Journal of Climate, 21(10), 2283-2296.

Vose, R. S., D. Arndt, V. F. Banzon, D. R. Easterling, B. Gleason, B. Huang, E. Kearns, J. H. Lawrimore, M. J. Menne, and T. C. Peterson (2012), NOAA's merged land–ocean surface temperature analysis, Bulletin of the American Meteorological Society, 93(11), 1677-1685.